Ultrafast Dynamics of a Red-Light-Activated Organic Photocatalyst in the Oxidative Hydroxylation of Phenylboronic Acid

Anshu Kumar[αβ], *Benjamin Thompson*[αγ], *Md Mubarak Hossain*[α], *Thomas L. Gianetti*[α], *Vanessa M. Huxter*[αβ*]

[α] Department of Chemistry and Biochemistry, University of Arizona, Tucson, Arizona 85721, United States

[β] Department of Physics, University of Arizona, Tucson, Arizona 85721, United States

[γ] College of Optical Sciences, University of Arizona, Tucson, Arizona 85721, United States

Corresponding Author

*vhuxter@arizona.edu

ABSTRACT

Over the past few years, photoredox catalysis has led to significant transformations in modern synthetic chemistry. It has allowed the development of new synthetic pathways for the assembly of complex molecular scaffolds using light as a driving force. However, investigations of the ultrafast light-initiated mechanisms required for these reactions are relatively scarce. Here we follow the ultrafast dynamics of a red-light organic photocatalyst, *N,N′*-di-*n*-propyl-1,13-dimethoxyquinacridinium (^{n}Pr-DMQA^{+}), in the aerobic oxidative hydroxylation of phenylboronic acid using transient absorption and time correlated single photon counting spectroscopy. Global target analysis supports a reaction mechanism that proceeds through the excited triplet state of ^{n}Pr-DMQA^{+}, leading to the generation of a superoxide anion and subsequent oxidative hydroxylation. The triplet pathway proposed here has relatively wide application in organic photocatalytic oxidative reactions including those using methylene blue and other organic dyes as catalysts. Observation of the ultrafast dynamics of ^{n}Pr-DMQA^{+} as it acts as a catalyst can provide insights to improve the efficiency of oxidative hydroxylation reactions and the mechanisms of photoredox catalysis more broadly.

TOC

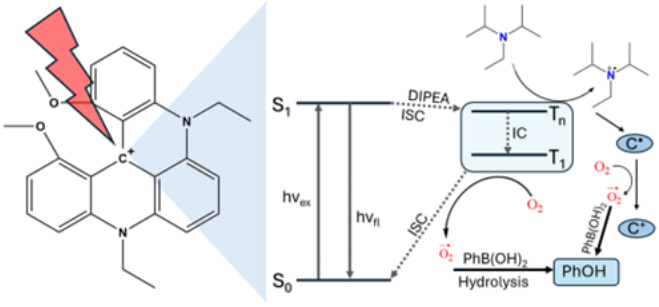

KEYWORDS Photoredox catalysis; organic photocatalyst; charge transfer; transient absorption; triplet state.

Introduction

Photoredox catalysis has been the subject of significant interest[1-11] due to its potential environmental and economic advantages.[12-15] Over the past decade, the growth of photoredox catalysis has significantly influenced chemical methodologies, enabling the development of new synthetic pathways through light activation,[7-9, 16-18] simplifying complex reactions under milder conditions,[3, 16, 19-22] minimizing the reliance on harmful reagents,[3, 23, 24] and enhancing waste reduction and process efficiency. While photoredox catalysis using transition metal

complexes allows access to a wide array of reactions,[7, 25-32] issues such as cost and potential toxicity persist. Organic photocatalysts have emerged as a potential solution due to their structural flexibility and low cost. Red-light-activated photoredox catalytic processes are an area of great interest.[33-38] The benefits of red-light photocatalysis include its lower energy requirement, reduced side reactions, minimized health risks, and its greater penetration through scattering media.[39-43]

This work investigates the ultrafast dynamics of the organic *N,N′*-di-*n*-propyl-1,13-dimethoxyquinacridinium (^{n}Pr-DMQA^{+}) red-light photocatalyst to understand its mechanism in the aerobic oxidative hydroxylation of phenylboronic acid. ^{n}Pr-DMQA^{+}, shown in Figure 1 inset, is a member of the helicene family characterized by a condensed aromatic structure, with fused rings arranged in a nonplanar fashion to alleviate steric hindrances.[44] This arrangement, combining a conjugated π-electron system with nonplanarity, is known to favor enhanced intersystem crossing rates.[44-47] Here we use transient absorption (TA) and time correlated single photon counting (TCSPC) to track the dynamics of the catalyst. These measurements suggest that the mechanism proceeds through a long-lived triplet state of ^{n}Pr-DMQA^{+}.

Experimental Section

^{n}Pr-DMQA^{+} with a BF_4^- counter ion was synthesized according to a previously reported method.[43] For all optical measurements, solutions were prepared by dissolving 2.5 mg of ^{n}Pr-DMQA^{+} in 5 mL of *N,N*-dimethylformamide (DMF). 0.5 mmol of phenylboronic acid and 1

mmol of *N,N*-Diisopropylethylamine (DIPEA) were added to ^{n}Pr-DMQA^{+} in DMF, to generate a previously reported oxidative hydroxylation reaction mixture.[42] Steady-state UV/Vis absorbance measurements were collected using an Agilent Cary 100. Fluorescence spectra were gathered using an Agilent Cary Eclipse. All measurements were performed at room temperature.

TCSPC data were collected using a previously described home-built system.[48] Briefly, the output of a Coherent Vitara Ti:Sapphire oscillator generating pulses of 100 fs at 800 nm was frequency-doubled to 400 nm through a type-I β-barium borate (BBO) crystal and focused into the sample to generate fluorescence. The fluorescence was then directed to a monochromator and photomultiplier tube detector and lifetime decays were measured using a SPC-130 TCSPC (Becker-Hickl).

Broadband-detected TA experiments were performed using a home-built apparatus. Our regenerative amplifier laser system (Libra, Coherent) delivered 100 fs pulses at 800 nm with an energy output of approximately 4 mJ per pulse at a frequency of 1kHz. For our experiments, we allocated 1.5 mJ from this output to create a broad spectrum of visible light. This was achieved by focusing the beam into an argon-filled tube generating white light that spanned 450 nm to 700 nm for broadband detection. The broadband pulses were temporally compressed using chirped mirrors (Laser Quantum). Following compression, the broadband light was split into pump and probe beams. The intensity of the pump beam was controlled using a variable neutral density filter, consisting of a waveplate and polarizer duo, before being shaped by a Dazzler (FASTLITE) pulse shaper. Post-shaping, the pump beam exhibited a uniform intensity

profile with a spectral range of 570 nm and 630 nm. The probe beam also passed through a variable neutral density filter and was delayed relative to the pump pulse using a mechanical delay line (DL325, Newport). The pump and probe were focused to the sample position using 150 mm and 100 mm focal length lenses, respectively, resulting in a focal spot size of 100 μm. The signal was collected using a SpectraPro HRS-300 spectrometer and a PIXIS 400 CCD camera (Princeton Instruments). To determine the temporal resolution of the pulses, a BBO crystal was utilized to generate a second harmonic signal for cross-correlation. This signal was measured using a silicon-based detector (Det10A2) from Thorlabs connected to a lock-in amplifier. The temporal width of the pulses was ~40 fs as shown in Figure S1 (see supporting information). The power at the sample position was approximately 50 nJ.

Result and Discussion

Figure 1 inset shows the structure of the helical carbenium ion, N,N′-di-n-propyl-1,13-dimethoxyquinacridinium (^{n}Pr-DMQA^{+}) with a BF_4^- counter ion. The steady state absorption spectrum of ^{n}Pr-DMQA^{+} in N, N-dimethylformamide (DMF) is presented in Figure 1. The main feature at 620 nm corresponds to the S_0 to S_1 with a shoulder around 585 nm[42, 49] associated with a vibrational mode. The fluorescence, shown in Figure 1, is maximized at 685 nm, corresponding to a Stoke shift of 0.2 eV.

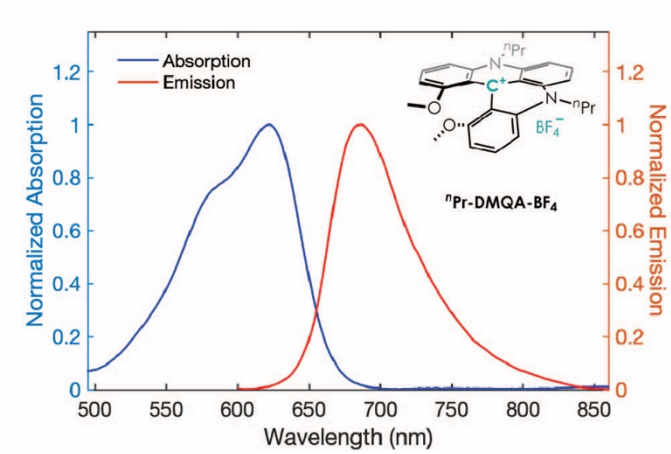

Figure 1. Normalized absorption (blue trace) and fluorescence (red trace) spectra of ^{n}Pr-DMQA^{+} dissolved in N, N-Dimethylformamide (DMF). Inset top right: structure of ^{n}Pr-DMQA^{+} with a BF_4^- counter ion. Carbon-bonded hydrogen atoms are omitted for clarity.

^{n}Pr-DMQA^{+} is used here to catalyze the oxidative hydroxylation reaction of phenylboronic acid (PhB(OH)$_2$) in the presence of DIPEA. DIPEA acts as a sacrificial amine while PhB(OH)$_2$ is the reagent. The absorption spectrum of ^{n}Pr-DMQA^{+} does not exhibit a spectral shift when in solution with either DIPEA, and/or PhB(OH)$_2$. However, the fluorescence is quenched by about 60% in the presence of DIPEA with no shift in the peak position of the emission (see Figure S2 in the supporting information). The presence of PhB(OH)$_2$ does not affect the ^{n}Pr-DMQA^{+} fluorescence.

Figure 2 presents TCSPC traces of ^{n}Pr-DMQA^{+} fluorescence in DMF with and without DIPEA. The recorded fluorescence lifetime of ^{n}Pr-DMQA^{+} is 5.8 ± 0.8 ns, which is unchanged

by the presence of $PhB(OH)_2$. In the presence of DIPEA, this lifetime is quenched to 2.0 ± 0.3 ns.

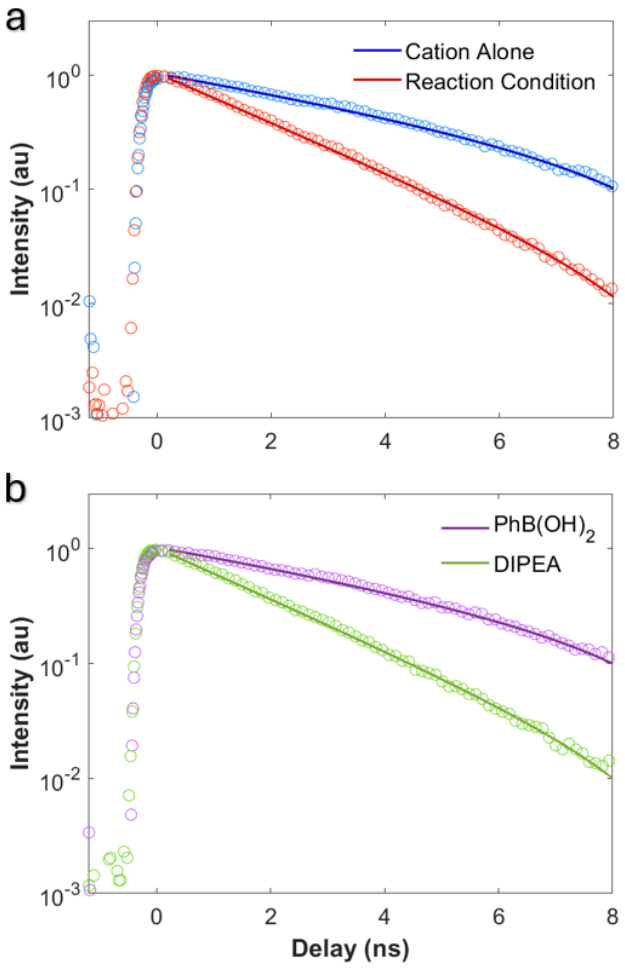

Figure 2. (a) Comparison between TCPSC data for ^{n}Pr-DMQA^{+} alone in DMF alone (blue) and in the presence of both DIPEA and $PhB(OH)_2$ in DMF (reaction condition, red). The solid traces show a single exponential fit to the corresponding data. (b) Comparison between the TCPSC data for ^{n}Pr-DMQA^{+} in the presence of $PhB(OH)_2$ (purple) and DIPEA (green). The solid traces of the respective colors show fits to the corresponding data. Both plots are on a semi-log scale.

TA data for ^{n}Pr-DMQA^{+} in DMF is presented in Figure 3a. A large ground state bleach (GSB) signal is observed around 625 nm immediately after pump excitation. This GSB signal exhibits red shift of ~16 meV by 150 ps. Complete recovery of this bleach was not achieved within the 1.4 ns maximum observation time of the measurements. Another bleach minimum feature centered at 585 nm exhibited a similar response. A third bleach feature associated with stimulated emission (SE) was also observed at 680 nm. Complete recovery of the bleach did not occur within the maximum delay time of the experiment, consistent with the TCSPC lifetime of 5.8 ± 0.8 ns.

The excited state absorption (ESA) feature that appears at wavelengths lower than 500 nm provides further insight into the ^{n}Pr-DMQA^{+} dynamics. An ESA centered at 485 nm shifted to 495 nm over the first 200 ps and then maintained most of its amplitude by the end of 1.4 ns experimental timespan. A gradually evolving ESA signal was observed around 530 nm, although this was initially obscured by the broad negative bleach. The signal changes sign around 100 ps, and reached its maximum positive amplitude around 300 ps. The slow rise and persistence of this signal beyond 1.4 ns suggests it originates from the S_1 state, potentially corresponding to transitions from S_1 to higher lying triplet states.[50]

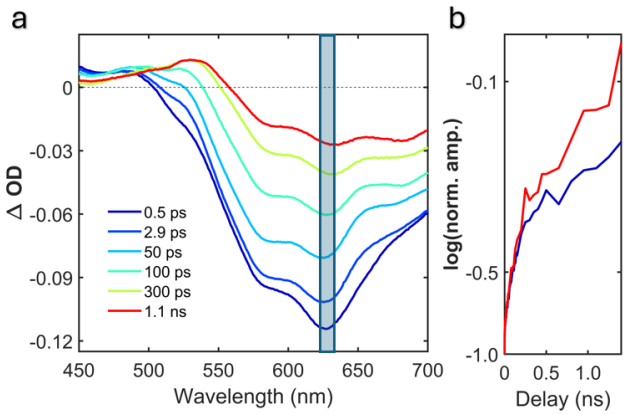

Figure 3. (a) TA traces of ^{n}Pr-DMQA^{+} in DMF at different delay times. (b) Comparison between the normalized traces produced after integrating the highlighted region in panel (a) highlighting the slower recovery of bleach for ^{n}Pr-DMQA^{+} alone in DMF (blue trace) in comparison to when DIPEA is present (red trace) in the solution with y-axis on log scale.

TA data for ^{n}Pr-DMQA^{+} in the presence of PhB(OH)$_2$ is shown in Figure S3 (see supporting information). The ultrafast dynamics of ^{n}Pr-DMQA^{+} are unchanged in the presence of PhB(OH)$_2$. TA data of ^{n}Pr-DMQA^{+} in DMF following excitation at 620 nm in the presence of DIPEA is shown in Figure S4 (see supporting information). Following pump excitation, a GSB feature centered around 625 nm is observed. This GSB undergoes a red shift of ~16 meV over 150 ps, consistent with that observed for the photocatalyst alone. The immediate photoinduced response is confirmed by the bleach minimum established within the instrument response time, accompanied by rapid recovery within 0.5 ps. Although the bleach did not fully recover over the experimental timescale, its recovery was faster compared to ^{n}Pr-DMQA^{+} with or

without $PhB(OH)_2$ (see Figure 3b), consistent with quenching in the presence of the amine. This observation of overall faster bleach recovery is consistent with the TCSPC measurement for ^{n}Pr-DMQA$^+$ in the presence of DIPEA shown in Figure 2b with a lifetime of 2.0 ± 0.3 ns. The ESA at ~485 nm is present immediately following pump excitation, while the other ESA feature emerges at ~530 nm after 100 ps, initially as part of the broad bleach feature and is possibly associated with transition from excited state to higher lying triplet state. Both ESA features persist throughout the maximum delay of the measurement, indicating a long-lived nature similar to that observed for ^{n}Pr-DMQA$^+$ alone.

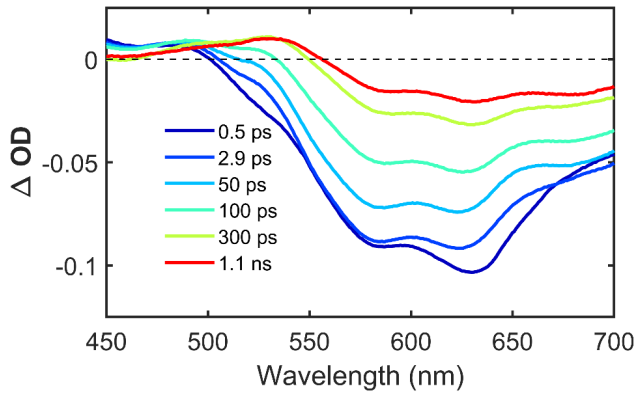

Figure 4. TA spectral traces of ^{n}Pr-DMQA$^+$ in the presence of DIPEA and $PhB(OH)_2$ in DMF at different delay times.

TA data of ^{n}Pr-DMQA$^+$ in DMF in the presence of DIPEA and $PhB(OH)_2$ is presented in Figure 4. The combination of DIPEA and $PhB(OH)_2$ at 100:50 ratios to that of ^{n}Pr-DMQA$^+$ in DMF corresponds to the previously demonstrated conditions for a photocatalytic oxidative

hydroxylation reaction.[42] The TA data shown in Figure 4 is similar to that of ^{n}Pr-DMQA^{+} alone although with faster bleach recovery, as observed in the case when only DIPEA is present (see Figure S4 in supporting information). The negative signal from 500 nm to 700 nm appears immediately following pump excitation. Within the negative feature there are three minima at ~685 nm, ~625 nm, and ~585 nm. GSB is observed around 625 nm post pump excitation, with a red shift of ~16 meV over 150 ps, consistent with that observed for the photocatalyst alone. The prompt photoinduced response is confirmed by the bleach minimum established within the instrument response time, accompanied by rapid recovery within 0.5 ps. Although the bleach does not fully recover over the experimental timescale, its recovery is faster compared to ^{n}Pr-DMQA^{+} with or without PhB(OH)$_2$, which is consistent with quenching in the presence of the amine (see Figure 3b). This observation of overall faster bleach recovery is consistent with the TCSPC measurement shown in Figure 2a, with a lifetime of 2.0 ± 0.3 ns, corresponding with quenching in the presence of the amine. Similar to previous observations, the ESA at ~485 nm is present following pump excitation, while the other ESA feature emerges around 530 nm after 100 ps, initially as part of the broad bleach feature. Both ESA features persist throughout the maximum delay of the measurement.

For all TA measurements presented here, we observe a broad negative signal extending from 500 nm to 700 nm, associated with GSB and SE. Moreover, characteristic bleach features associated with SE and GSB are consistently observed around 685 nm, 625 nm, and 585 nm, respectively. Additionally, we observe ESA signals around 485 nm and 530 nm, which persist throughout the experimental timescale. However, notable differences arise in the overall

recovery dynamics of the bleach features at longer delay times. In the presence of DIPEA and for the reaction conditions with both DIPEA and $PhB(OH)_2$, the recovery of the negative signal between 580 nm and 700 nm is faster compared to ^{n}Pr-DMQA^{+} alone, supporting the effect of amine quenching on the excited state lifetime. In addition, the presence of $PhB(OH)_2$ does not alter the dynamics of the ^{n}Pr-DMQA^{+} cation (see Figure S3 in supporting information).

To analyze the TA data, we have constructed a kinetic model building upon prior investigations into helicenes, in particular, pathways involving intersystem crossing to triplet states,[45, 47, 51-54] which can be enhanced in nonplanar aromatic molecules.[44, 46, 55] Target analysis of the TA data was conducted based on the model depicted in Figure 5c using Python-based package, KIMOPACK.[56] In all cases, the best fit to the data was achieved by considering a total of five decay rates, with the rate for intersystem crossing from the triplet state to the singlet ground state held as an offset due to its microsecond timescale[44, 45, 53, 57] which is significantly longer than the maximum delay time of the TA experiments.

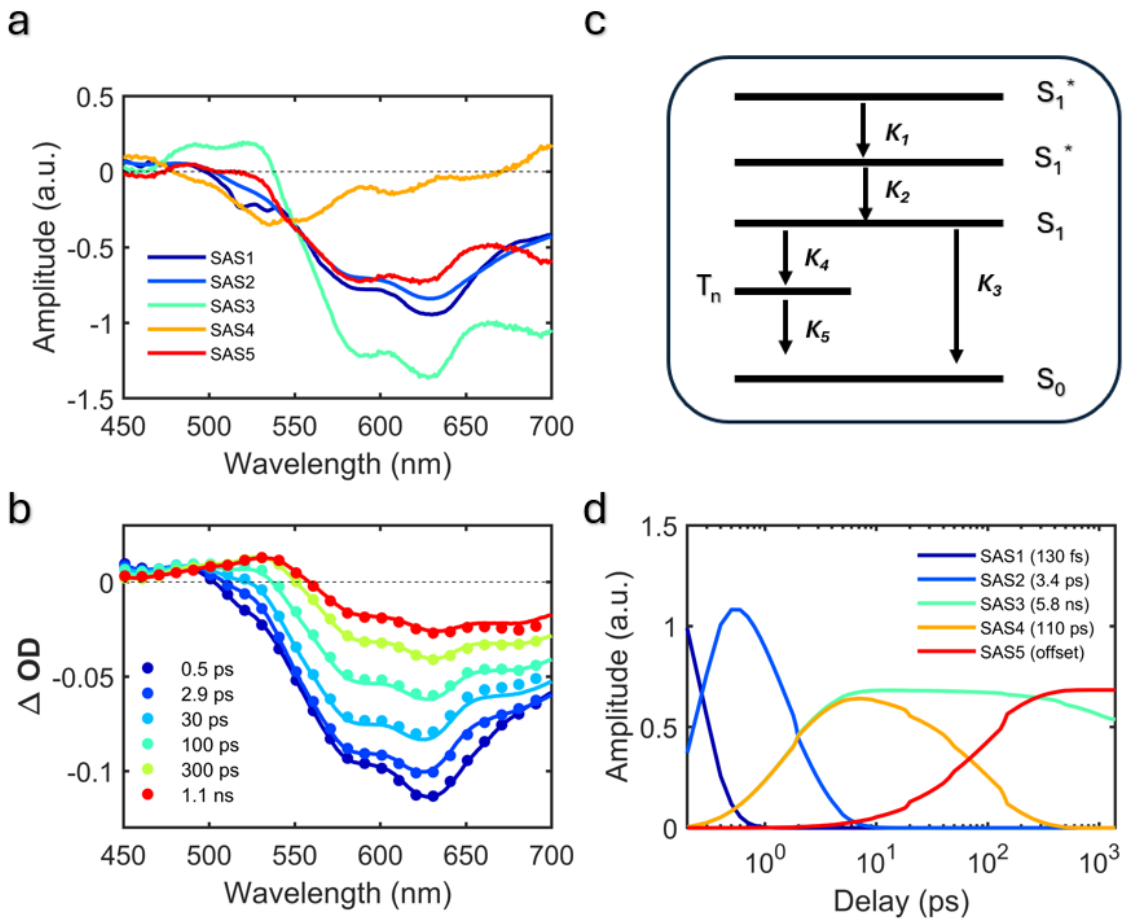

Figure 5. (a) Species-associated spectra (SAS) from the targeted analysis using the model shown in panel (c), and (b) raw TA data (dots) and fit (solid traces) for ^{n}Pr-DMQA^{+} in DMF. (c) Kinetic model used in the target analysis with (d) corresponding kinetics for the model with the delay axis on log-scale.

Spectral analysis of the TA data reveals distinct features across the five species-associated spectra (SAS). Figure 5 presents the results for ^{n}Pr-DMQA^{+} alone in DMF. The first three SAS exhibit a bleach minimum centered around the ground state bleach (GSB) minimum at 625

nm, accompanied by a shoulder at 585 nm, corresponding to a vibronic sub-band observed in the absorption spectrum. The first two SAS display similar spectral characteristics. SAS1 undergoes decay within 130 ± 60 fs (all error estimates based on a 95% confidence interval), attributed to solvent-induced vibrational cooling. It is accompanied by positive amplitude below 500 nm, corresponding to ESA to higher-lying S_n states. In contrast, SAS2 decays over a longer timescale of 3.4 ± 0.5 ps, attributed to intramolecular vibrational redistribution (IVR). SAS3, corresponding to a time constant of 5.8 ns consistent with our TCSPC results, has another local minimum beyond 660 nm related to SE and represents the S_1 to S_0 decay along with residual GSB. We assign SAS4 to ISC from the excited singlet state to the triplet manifold, with an associated timescale of 110 ± 18 ps.[58-62] Spectrally centered around 530 nm, this component has a local minimum around 620 nm, associated with GSB. Previous reports on azahelicenes compounds have indicated a typical S_1-T_1 energy gap to be more than 0.5 eV.[44, 52] This is consistent with the absence of phosphorescence observed up to 900 nm at cryogenic temperatures for ^{n}Pr-DMQA^{+} (see Figure S5 in supporting information).

Given the timescale associated with ISC in this system, the population of the S_1 state may initially transition to a higher-lying T_n state, followed by rapid internal conversion to T_1 and subsequent return to the S_0 ground state. This sequence has been reported previously for aza[7]helicene and other conjugated systems.[47, 55] Ultrafast ISC has been previously observed in organic molecules,[58, 60, 61, 63-66] despite the absence of heavy atoms. This phenomenon has been attributed to the very small energy difference between the excited S_1 and T_n states.[58, 60-62] Reports also highlight enhanced spin-orbit coupling in nonplanar aromatic compounds, which

facilitates transitions between states with different spin.[44, 46, 62, 65] The amplitude of SAS5 is similar to that of SAS1 and SAS2 (see Figure 5a). We proposed that it is associated with ISC from T_1 to S_0. This non-decaying offset is consistent with the long lifetimes associated with such transitions.[44, 45, 53, 57]

The results of the target analysis on the TA data for ^{n}Pr-DMQA^{+} and PhB(OH)$_2$ in DMF are the same as those of the cation alone, indicating that the acid does not influence the photocatalyst dynamics (see Table S1 in supporting information). Figure 6 summarizes these results and compares them with the raw TA data. All the SAS are associated with the same components as in the case of the photocatalyst alone in DMF and have similar timescales. As before, SAS1 and SAS2 follow each other, while SAS3 shows bleach near 680 nm consistent with emission from the photocatalyst. SAS4 remains unchanged from the previous case when only the photocatalyst is present in DMF, while SAS5 represents an offset associated with the transition from T_1 to S_0 state.

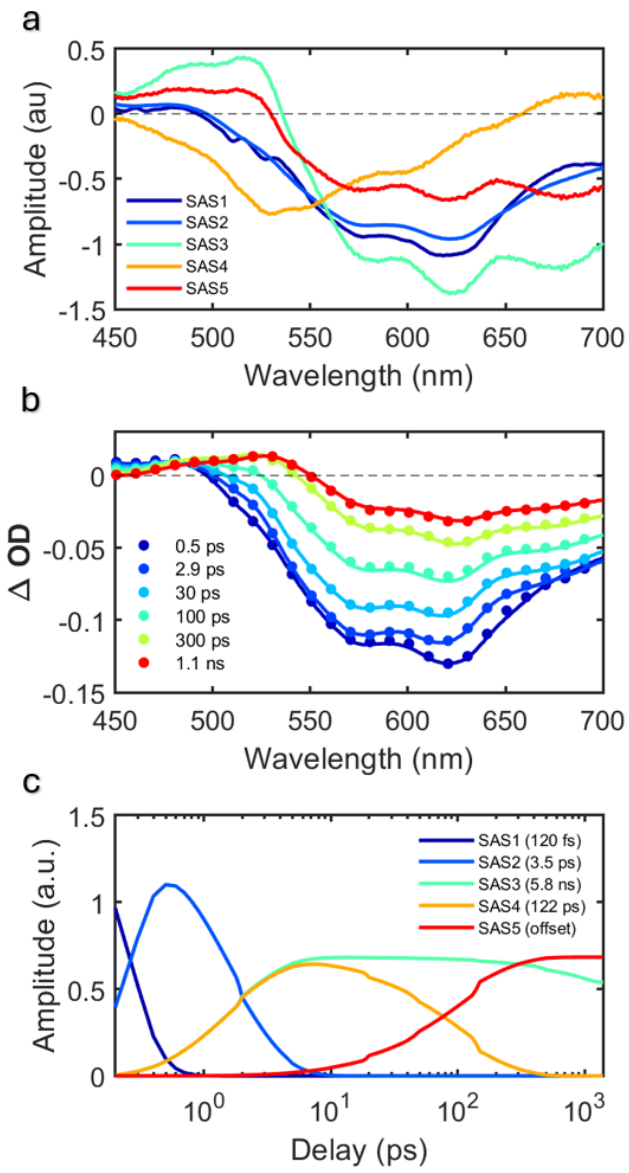

Figure 6. (a) SAS from the target analysis based on the model shown in Figure 5c and (b) raw TA data (dots) and fit (solid traces) for ^{n}Pr-DMQA^{+} in the presence of PhB(OH)$_2$ in DMF and (c) corresponding kinetics with the delay axis on log-scale.

Target analysis of the TA data for ^{n}Pr-DMQA^{+} in DMF in the presence of DIPEA is summarized in Figure 7. The lifetimes of SAS1 and SAS2 remain nearly unchanged at 112 ± 60 fs and 3.3 ± 0.6 ps, respectively, with bleach minima situated around 625 nm, mirroring those of ^{n}Pr-DMQA^{+} alone. SAS3, with a lifetime of 2.0 ns (consistent with TCSPC measurements shown in Figure 2b, exhibits excited state quenching in the presence of amine. This is attributed to the introduction of additional non-radiative decay pathways.[67-69] SAS4 (assigned to ISC) has approximately the same timescale (110 ± 18 ps) as in the data for the cation alone but shows significant change in the spectral distribution. This includes a bleach minimum shift from 530 nm to 570 nm and a pronounced bleach near 610 nm. The observed quenching of the S_1 lifetime by the amine likely facilitates ISC to the triplet state.[69] This is suggested by the increased relative amplitude of SAS4 (Figure 7a) associated with an enhanced population transfer to the triplet state. After the triplet state is populated, an electron transfer occurs from the amine to this excited state as has been previously observed in other organic molecules.[69-74] This is further supported by the difference observed in the spectral profile of SAS5, an offset associated with the transition from T_1 to S_0, with diminished amplitude in comparison to SAS1 and SAS2 (Figure 7a).

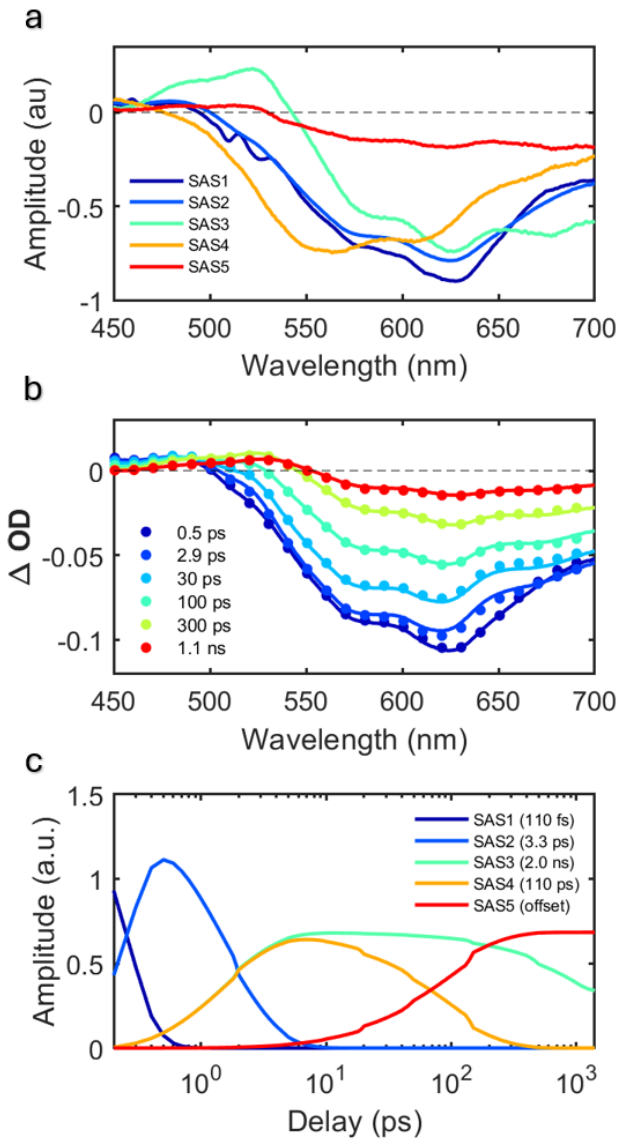

Figure 7. (a) SAS from the targeted analysis and (b) raw TA data (dots) and fit (solid traces) for ^{n}Pr-DMQA^{+} in the presence of DIPEA in DMF and (c) corresponding kinetics with the delay axis on log-scale.

Global target analysis of the TA data for ^{n}Pr-DMQA^{+} in DMF in the presence of PhB(OH)$_2$, and DIPEA presented in Figure 8 is consistent with the results from the analysis of the TA data

for ^{n}Pr-DMQA^{+} and DIPEA shown in Figure 7. The lifetimes associated with SAS1 and SAS2 are similar to those observed for ^{n}Pr-DMQA^{+} in DMF, which indicates that solvation and IVR processes are not significantly modified by the presence of DIPEA or $PhB(OH)_2$ (see Table S2 in supporting information). SAS3, has a 2.0 ns timescale consistent with the TCSPC measurements shown in Figure 2a. SAS4, with a 112 ± 21 ps lifetime, has the same spectral profile as shown in Figure 7a where DIPEA is present. This suggests that there is enhanced population transfer to the triplet state.[69] Finally, SAS5, an offset associated with the transition from T_1 to S_0, has a lower amplitude compared to the first 3 SAS, consistent with the behavior in the presence of DIPEA alone (Figure 7a) when juxtaposed to the relative amplitude of SAS5 with respect to SAS1 and SAS2 in the cases of the cation alone in DMF or when the reagent $PhB(OH)_2$ is also present (Figure 5a and 6a). This suggests a depletion of the triplet state.

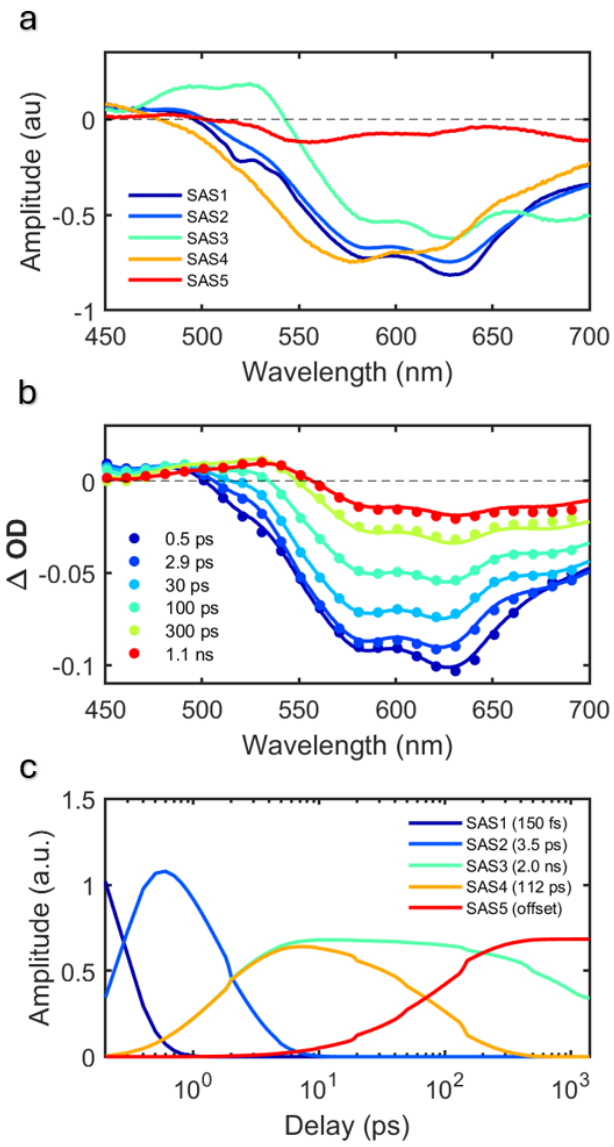

Figure 8. (a) SAS from the targeted analysis based on the model shown in Figure 5c, and (b) raw TA data (dots) and fit (solid traces) for ^{n}Pr-DMQA^{+} in the presence of DIPEA and phenylboronic acid in DMF and (d) corresponding kinetics for the model with the delay axis on log-scale.

Analysis of the TA and TCSPC data suggests that the aerobic hydroxylation of $PhB(OH)_2$ by ^{n}Pr-DMQA^{+} proceeds through the triplet state as shown in Figure 9. The process begins with excitation to the S_1 state, followed by vibrational cooling and solvent reorganization. The system returns to the ground state either by radiative or non-radiative transitions from S_1 to S_0 or through ISC to triplet states followed by another ISC process from T_1 to S_0. The ISC process from S_1 to T_n is enhanced in the presence of DIPEA and is associated with the quenching of the radiative lifetime. Kinetic analysis of the TA data supports the presence of a rapid ISC process to a higher-lying triplet state, which is close in energy to S_1.[60, 61, 64] Enhanced spin-orbit coupling can be associated with a nonplanar aromatic molecular structure, with the magnitude of the enhancement being directly proportional to the deviation from planarity.[44, 46] This phenomenon has been previously observed in studies of aza[7]helicene, where the rate of ISC from S_1 to T_3 was found to be three orders of magnitude faster than that from S_1 to T_1.[55] A similar trend has been observed for 4-dimethylaminochalcone, showing an ISC rate significantly exceeding the radiative transition.[64] Electron transfer from DIPEA ($^{i}Pr_2NEt/^{i}Pr_2NEt^{\bullet+}$ = +0.72 V vs SCE in DMF) to an excited triplet state ($E_{1/2}(C^{+}*/C^{\bullet})$ = +1.18 V vs SCE in DMF) [43, 69-73] can then lead to the formation of the ground state neutral ^{n}Pr-DMQA radical which can subsequently reduce oxygen to superoxide radical anion under aerobic conditions.[75] Alternatively an oxidative pathway is also viable if the excited triplet state of the cationic ^{n}Pr-DMQA ($E_{1/2}$ ($C^{\bullet++}/C^{+}*$) = −0.62 V vs SCE in DMF) is oxidized under aerobic condition ($O_2/O_2^{\bullet-}$ = –0.57 V vs SCE in DMF[43]) generating dicationic radical species of the ^{n}Pr-DMQA and the superoxide radical anion. Both pathways are thermodynamically feasible. In

either case, the superoxide radical anion can then react with $PhB(OH)_2$, producing phenol through a subsequent hydrolysis step.

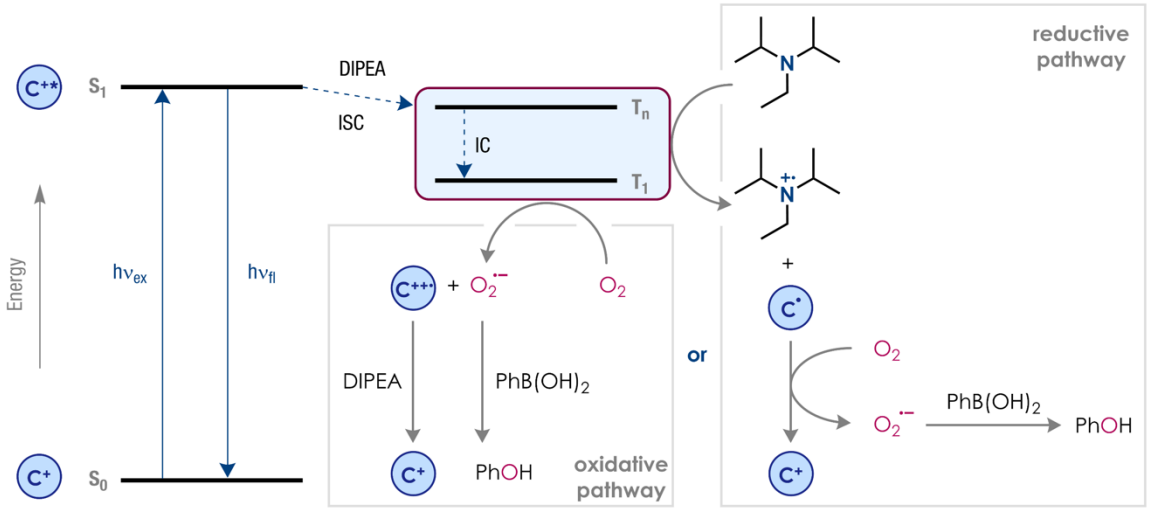

Figure 9. Mechanism for hydroxylation of $PhB(OH)_2$ to phenol using ^{n}Pr-DMQA$^+$ as a photoredox catalyst. DIPEA enhances the triplet population of photocatalyst due to formation of a radical ion-pair which is facilitated by electron transfer from the amine to the triplet state of the photocatalyst. Alternatively, O_2 in solution can react with the ^{n}Pr-DMQA$^+$ triplet state to form $O_2^{\bullet-}$. The oxidative reaction of $O_2^{\bullet-}$ with $PhB(OH)_2$ and subsequent hydrolysis results in the production of phenol.

Conclusion

Steady-state absorption, fluorescence spectroscopy, TCSPC, and TA data were used to study the mechanism of ^{n}Pr-DMQA$^+$ acting as a photoredox catalyst for the oxidative hydroxylation of $PhB(OH)_2$. While the absorption of ^{n}Pr-DMQA$^+$ in DMF was insensitive to the presence of

either DIPEA or $PhB(OH)_2$, the fluorescence was quenched by DIPEA. TA measurements tracked the ultrafast dynamics, revealing features consistent with rapid relaxation processes such as solvent reorganization and IVR, as well as longer-lived singlet and triplet excited states. Global target analysis of the TA data suggests that ISC is enhanced in the presence of DIPEA. This facilitates the formation of a long-lived triplet state which then can generate superoxide radical anion in two analogous pathways. This superoxide radical anion, in turn, interacts with $PhB(OH)_2$, leading to the production of phenol.

Supporting Information. Supplemental spectroscopic data including pulse characterization, steady-state fluorescence, and additional transient absorption data.

Author Information. The authors declare no competing financial interests.

Acknowledgment. V. M. H. gratefully acknowledges support from the donors of the American Chemical Society Petroleum Research Fund through grant no. 65536-ND6 and from the National Science Foundation through CAREER award grant no. 2236610. T. L. G. acknowledges support from the National Science Foundation through CAREER award grant no. 2144018.

References

(1) Védrine, J. C. Metal Oxides in Heterogeneous Oxidation Catalysis: State of the Art and Challenges for a More Sustainable World. *ChemSusChem* **2019**, *12* (3), 577-588. DOI: doi.org/10.1002/cssc.201802248.
(2) Thomas, J. M.; Thomas, W. J. *Principles and Practice of Heterogeneous Catalysis*; John Wiley & Sons, 2014.
(3) Romero, N. A.; Nicewicz, D. A. Organic Photoredox Catalysis. *Chem. Rev.* **2016**, *116* (17), 10075-10166. DOI: 10.1021/acs.chemrev.6b00057.
(4) Jiang, W.; Low, B. Q. L.; Long, R.; Low, J.; Loh, H.; Tang, K. Y.; Chai, C. H. T.; Zhu, H.; Zhu, H.; Li, Z.; et al. Active Site Engineering on Plasmonic Nanostructures for Efficient Photocatalysis. *ACS Nano* **2023**, *17* (5), 4193-4229. DOI: 10.1021/acsnano.2c12314.
(5) Liu, J.; Ye, L.; Wooh, S.; Kappl, M.; Steffen, W.; Butt, H.-J. Optimizing Hydrophobicity and Photocatalytic Activity of PDMS-Coated Titanium Dioxide. *ACS Appl. Mater. Interfaces* **2019**, *11* (30), 27422-27425. DOI: 10.1021/acsami.9b07490.
(6) Goddard, J.-P.; Ollivier, C.; Fensterbank, L. Photoredox Catalysis for the Generation of Carbon Centered Radicals. *Acc. Chem. Res.* **2016**, *49* (9), 1924-1936. DOI: 10.1021/acs.accounts.6b00288.
(7) Prier, C. K.; Rankic, D. A.; MacMillan, D. W. C. Visible Light Photoredox Catalysis with Transition Metal Complexes: Applications in Organic Synthesis. *Chem. Rev.* **2013**, *113* (7), 5322-5363. DOI: 10.1021/cr300503r.
(8) Hopkinson, M. N.; Tlahuext-Aca, A.; Glorius, F. Merging Visible Light Photoredox and Gold Catalysis. *Acc. Chem. Res.* **2016**, *49* (10), 2261-2272. DOI: 10.1021/acs.accounts.6b00351.
(9) Lang, X.; Zhao, J.; Chen, X. Cooperative Photoredox Catalysis. *Chem. Soc. Rev.* **2016**, *45* (11), 3026-3038. DOI: 10.1039/C5CS00659G.
(10) Shaw, M. H.; Twilton, J.; MacMillan, D. W. C. Photoredox Catalysis in Organic Chemistry. *J. Org. Chem.* **2016**, *81* (16), 6898-6926. DOI: 10.1021/acs.joc.6b01449.
(11) Wang, C.-S.; Dixneuf, P. H.; Soulé, J.-F. Photoredox Catalysis for Building C–C Bonds from C(sp2)–H Bonds. *Chem. Rev.* **2018**, *118* (16), 7532-7585. DOI: 10.1021/acs.chemrev.8b00077.
(12) Anastas, P. T.; Kirchhoff, M. M. Origins, Current Status, and Future Challenges of Green Chemistry. *Acc. Chem. Res.* **2002**, *35* (9), 686-694. DOI: 10.1021/ar010065m.
(13) Liu, J.; Dietz, T.; Carpenter, S. R.; Alberti, M.; Folke, C.; Moran, E.; Pell, A. N.; Deadman, P.; Kratz, T.; Lubchenco, J.; et al. Complexity of Coupled Human and Natural Systems. *Science* **2007**, *317* (5844), 1513-1516. DOI: 10.1126/science.1144004.
(14) Clarke, C. J.; Tu, W.-C.; Levers, O.; Bröhl, A.; Hallett, J. P. Green and Sustainable Solvents in Chemical Processes. *Chem. Rev.* **2018**, *118* (2), 747-800. DOI: 10.1021/acs.chemrev.7b00571.

(15) Liu, J.; Mooney, H.; Hull, V.; Davis, S. J.; Gaskell, J.; Hertel, T.; Lubchenco, J.; Seto, K. C.; Gleick, P.; Kremen, C.; et al. Systems Integration for Global Sustainability. *Science* **2015**, *347* (6225), 1258832. DOI: 10.1126/science.1258832.
(16) Ravelli, D.; Fagnoni, M.; Albini, A. Photoorganocatalysis. What for? *Chem. Soc. Rev.* **2013**, *42* (1), 97-113. DOI: 10.1039/C2CS35250H.
(17) Skubi, K. L.; Blum, T. R.; Yoon, T. P. Dual Catalysis Strategies in Photochemical Synthesis. *Chem. Rev.* **2016**, *116* (17), 10035-10074. DOI: 10.1021/acs.chemrev.6b00018.
(18) Marzo, L.; Pagire, S. K.; Reiser, O.; König, B. Visible-Light Photocatalysis: Does It Make a Difference in Organic Synthesis? *Angew. Chem. Int. Ed.* **2018**, *57* (32), 10034-10072. DOI: 10.1002/anie.201709766.
(19) Xuan, J.; Feng, Z.-J.; Duan, S.-W.; Xiao, W.-J. Room Temperature Synthesis of Isoquino[2,1-a][3,1]oxazine and Isoquino[2,1-a]pyrimidine Derivatives via Visible Light Photoredox Catalysis. *RSC Adv.* **2012**, *2* (10), 4065-4068. DOI: 10.1039/C2RA20403G.
(20) Nicewicz, D. A.; Nguyen, T. M. Recent Applications of Organic Dyes as Photoredox Catalysts in Organic Synthesis. *ACS Catal.* **2014**, *4* (1), 355-360. DOI: 10.1021/cs400956a.
(21) Phelan, J. P.; Lang, S. B.; Compton, J. S.; Kelly, C. B.; Dykstra, R.; Gutierrez, O.; Molander, G. A. Redox-Neutral Photocatalytic Cyclopropanation via Radical/Polar Crossover. *J. Am. Chem. Soc.* **2018**, *140* (25), 8037-8047. DOI: 10.1021/jacs.8b05243.
(22) Shang, T.-Y.; Lu, L.-H.; Cao, Z.; Liu, Y.; He, W.-M.; Yu, B. Recent Advances of 1,2,3,5-Tetrakis(carbazol-9-yl)-4,6-dicyanobenzene (4CzIPN) in Photocatalytic Transformations. *Chem. Comm.* **2019**, *55* (38), 5408-5419. DOI: 10.1039/C9CC01047E.
(23) Hari, D. P.; König, B. Eosin Y Catalyzed Visible Light Oxidative C–C and C–P bond Formation. *Org. Lett.* **2011**, *13* (15), 3852-3855. DOI: 10.1021/ol201376v.
(24) Cantillo, D.; de Frutos, O.; Rincón, J. A.; Mateos, C.; Kappe, C. O. Continuous Flow α-Trifluoromethylation of Ketones by Metal-Free Visible Light Photoredox Catalysis. *Org. Lett.* **2014**, *16* (3), 896-899. DOI: 10.1021/ol403650y.
(25) Juris, A.; Balzani, V.; Belser, P.; von Zelewsky, A. Characterization of the Excited State Properties of Some New Photosensitizers of the Ruthenium (Polypyridine) Family. *Helvetica Chimica Acta* **1981**, *64* (7), 2175-2182. DOI: 10.1002/hlca.19810640723.
(26) Kalyanasundaram, K. Photophysics, Photochemistry and Solar Energy Conversion with Tris(bipyridyl) Ruthenium(II) and Its Analogues. *Coord. Chem. Rev.* **1982**, *46*, 159-244. DOI: 10.1016/0010-8545(82)85003-0.
(27) Bolm, C.; Beller, M. *Transition Metals for Organic Synthesis*; Wiley-VCH, Weinheim, 2004.
(28) Lowry, M. S.; Goldsmith, J. I.; Slinker, J. D.; Rohl, R.; Pascal, R. A.; Malliaras, G. G.; Bernhard, S. Single-Layer Electroluminescent Devices and Photoinduced Hydrogen Production from an Ionic Iridium(III) Complex. *Chem. Mat.* **2005**, *17* (23), 5712-5719. DOI: 10.1021/cm051312.
(29) Schultz, D. M.; Yoon, T. P. Solar Synthesis: Prospects in Visible Light Photocatalysis. *Science* **2014**, *343* (6174), 1239176. DOI: doi:10.1126/science.1239176.

(30) Kelly, C. B.; Patel, N. R.; Primer, D. N.; Jouffroy, M.; Tellis, J. C.; Molander, G. A. Preparation of Visible-Light-Activated Metal Complexes and Their Use in Photoredox/Nickel Dual Catalysis. *Nat. Protoc.* **2017**, *12* (3), 472-492. DOI: 10.1038/nprot.2016.176.
(31) Parasram, M.; Gevorgyan, V. Visible Light-Induced Transition Metal-Catalyzed Transformations: Beyond Conventional Photosensitizers. *Chem. Soc. Rev.* **2017**, *46* (20), 6227-6240. DOI: 10.1039/C7CS00226B.
(32) Twilton, J.; Le, C.; Zhang, P.; Shaw, M. H.; Evans, R. W.; MacMillan, D. W. C. The Merger of Transition Metal and Photocatalysis. *Nat. Rev. Chem.* **2017**, *1* (7), 0052. DOI: 10.1038/s41570-017-0052.
(33) Cocquet, G.; Ferroud, C.; Guy, A. A Mild and Efficient Procedure for Ring-Opening Reactions of Piperidine and Pyrrolidine Derivatives by Single Electron Transfer Photooxidation. *Tetrahedron* **2000**, *56* (19), 2975-2984. DOI: 10.1016/S0040-4020(00)00048-X.
(34) Cocquet, G.; Ferroud, C.; Simon, P.; Taberna, P.-L. Single Electron Transfer Photoinduced Oxidation of Piperidine and Pyrrolidine Derivatives to the Corresponding Lactams. *J. Chem. Soc. Perk. T. 2* **2000**, (6), 1147-1153. DOI: 10.1039/B001036G.
(35) Lee, J.; Papatzimas, J. W.; Bromby, A. D.; Gorobets, E.; Derksen, D. J. Thiaporphyrin-Mediated Photocatalysis Using Red Light. *RSC Adv.* **2016**, *6* (64), 59269-59272. DOI: 10.1039/C6RA11374E.
(36) Matsuzaki, K.; Hiromura, T.; Tokunaga, E.; Shibata, N. Trifluoroethoxy-Coated Subphthalocyanine affects Trifluoromethylation of Alkenes and Alkynes even under Low-Energy Red-Light Irradiation. *ChemistryOpen* **2017**, *6* (2), 226-230. DOI: 10.1002/open.201600172.
(37) Ravetz, B. D.; Pun, A. B.; Churchill, E. M.; Congreve, D. N.; Rovis, T.; Campos, L. M. Photoredox Catalysis Using Infrared Light via Triplet Fusion Upconversion. *Nature* **2019**, *565* (7739), 343-346. DOI: 10.1038/s41586-018-0835-2.
(38) Yerien, D. E.; Cooke, M. V.; García Vior, M. C.; Barata-Vallejo, S.; Postigo, A. Radical Fluoroalkylation Reactions of (Hetero)arenes and Sulfides Under Red Light Photocatalysis. *Org. Biomol. Chem.* **2019**, *17* (15), 3741-3746. DOI: 10.1039/C9OB00486F.
(39) Fülöp, A.; Peng, X.; Greenberg, M. M.; Mokhir, A. Nucleic Acid-Directed, Red Light-Induced Chemical Reaction. *Chem. Comm.* **2010**, *46* (31), 5659-5661. DOI: 10.1039/C0CC00744G.
(40) Carling, C.-J.; Olejniczak, J.; Foucault-Collet, A.; Collet, G.; Viger, M. L.; Nguyen Huu, V. A.; Duggan, B. M.; Almutairi, A. Efficient Red Light Photo-Uncaging of Active Molecules in Water upon Assembly into Nanoparticles. *Chem. Sci.* **2016**, *7* (3), 2392-2398. DOI: 10.1039/C5SC03717D.
(41) Zhang, H.; Trout, W. S.; Liu, S.; Andrade, G. A.; Hudson, D. A.; Scinto, S. L.; Dicker, K. T.; Li, Y.; Lazouski, N.; Rosenthal, J.; et al. Rapid Bioorthogonal Chemistry Turn-on through Enzymatic or Long Wavelength Photocatalytic Activation of Tetrazine Ligation. *J. Am. Chem. Soc.* **2016**, *138* (18), 5978-5983. DOI: 10.1021/jacs.6b02168.

(42) Mei, L.; Veleta, J. M.; Gianetti, T. L. Helical Carbenium Ion: A Versatile Organic Photoredox Catalyst for Red-Light-Mediated Reactions. *Journal of the American Chemical Society* **2020**, *142* (28), 12056-12061. DOI: 10.1021/jacs.0c05507.
(43) Hossain, M. M.; Shaikh, A. C.; Kaur, R.; Gianetti, T. L. Red Light–Blue Light Chromoselective C(sp2)–X Bond Activation by Organic Helicenium-Based Photocatalysis. *J. Am. Chem. Soc.* **2024**, *146* (12), 7922-7930. DOI: 10.1021/jacs.3c13380.
(44) Schmidt, K.; Brovelli, S.; Coropceanu, V.; Beljonne, D.; Cornil, J.; Bazzini, C.; Caronna, T.; Tubino, R.; Meinardi, F.; Shuai, Z.; et al. Intersystem Crossing Processes in Nonplanar Aromatic Heterocyclic Molecules. *J. Phys. Chem. A* **2007**, *111* (42), 10490-10499. DOI: 10.1021/jp075248q.
(45) Sapir, M.; Donckt, E. V. Intersystem Crossing in the Helicenes. *Chem. Phys. Lett.* **1975**, *36* (1), 108-110. DOI: 10.1016/0009-2614(75)85698-3.
(46) Nijegorodov, N. I.; Downey, W. S. The Influence of Planarity and Rigidity on the Absorption and Fluorescence Parameters and Intersystem Crossing Rate Constant in Aromatic Molecules. *J. Phys. Chem.* **1994**, *98* (22), 5639-5643. DOI: 10.1021/j100073a011.
(47) Beljonne, D.; Shuai, Z.; Pourtois, G.; Bredas, J. L. Spin–Orbit Coupling and Intersystem Crossing in Conjugated Polymers: A Configuration Interaction Description. *J. Phys. Chem. A* **2001**, *105* (15), 3899-3907. DOI: 10.1021/jp010187w.
(48) Swain, A.; Cho, B.; Gautam, R.; Curtis, C. J.; Tomat, E.; Huxter, V. Ultrafast Dynamics of Tripyrrindiones in Solution Mediated by Hydrogen-Bonding Interactions. *J. Phys. Chem. B* **2019**, *123* (26), 5524-5535. DOI: 10.1021/acs.jpcb.9b01916.
(49) Laursen, B. W.; Krebs, F. C. Synthesis of a Triazatriangulenium Salt. *Angew. Chem. Int. Ed.* **2000**, *39* (19), 3432-3434. DOI: 10.1002/1521-3773(20001002)39:19<3432::AID-ANIE3432>3.0.CO;2-S.
(50) Dean, J. C.; Oblinsky, D. G.; Rather, S. R.; Scholes, G. D. Methylene Blue Exciton States Steer Nonradiative Relaxation: Ultrafast Spectroscopy of Methylene Blue Dimer. *J. Phys. Chem. B* **2016**, *120* (3), 440-454. DOI: 10.1021/acs.jpcb.5b11847.
(51) Birks, J. B.; Birch, D. J. S.; Cordemans, E.; Vander Donckt, E. Fluorescence of the Higher Helicenes. *Chem. Phys. Lett.* **1976**, *43* (1), 33-36. DOI: 10.1016/0009-2614(76)80750-6.
(52) Graule, S.; Rudolph, M.; Shen, W.; Williams, J. A. G.; Lescop, C.; Autschbach, J.; Crassous, J.; Réau, R. Assembly of π-Conjugated Phosphole Azahelicene Derivatives into Chiral Coordination Complexes: An Experimental and Theoretical Study. *Chem. Eur. J.* **2010**, *16* (20), 5976-6005. DOI: 10.1002/chem.200903234.
(53) Anger, E.; Rudolph, M.; Norel, L.; Zrig, S.; Shen, C.; Vanthuyne, N.; Toupet, L.; Williams, J. A. G.; Roussel, C.; Autschbach, J.; et al. Multifunctional and Reactive Enantiopure Organometallic Helicenes: Tuning Chiroptical Properties by Structural Variations of Mono- and Bis(platinahelicene)s. *Chem. Eur. J.* **2011**, *17* (50), 14178-14198. DOI: 10.1002/chem.201101866.
(54) Koli, M.; Gupta, S.; Chakraborty, S.; Ghosh, A.; Ghosh, R.; Wadawale, A. P.; Ghanty, T. K.; Patro, B. S.; Mula, S. Design and Synthesis of BODIPY-Hetero[5]helicenes as Heavy-

Atom-Free Triplet Photosensitizers for Photodynamic Therapy of Cancer. *Chem. Eur. J.* **2023**, *29* (57), e202301605. DOI: 10.1002/chem.202301605.
(55) Liu, Y.; Aranda, D.; Santoro, F. A Computational Study of the Vibronic Effects on the Electronic Spectra and the Photophysics of Aza[7]helicene. *Phys. Chem. Chem. Phys.* **2021**, *23* (31), 16551-16563. DOI: 10.1039/D1CP00822F.
(56) Müller, C.; Pascher, T.; Eriksson, A.; Chabera, P.; Uhlig, J. KiMoPack: A python Package for Kinetic Modeling of the Chemical Mechanism. *J. Phys. Chem. A* **2022**, *126* (25), 4087-4099. DOI: 10.1021/acs.jpca.2c00907.
(57) Chen, J.; Cesario, T. C.; Rentzepis, P. M. Time-Resolved Spectroscopic Studies of Methylene Blue and Phenothiazine Derivatives Used for Bacteria Inactivation. *Chem. Phys. Lett.* **2010**, *498* (1), 81-85. DOI: 10.1016/j.cplett.2010.08.042.
(58) Reichardt, C.; Vogt, R. A.; Crespo-Hernández, C. E. On the Origin of Ultrafast Nonradiative Transitions in Nitro-Polycyclic Aromatic Hydrocarbons: Excited-State Dynamics in 1-Nitronaphthalene. *J. Chem. Phys.* **2009**, *131* (22). DOI: 10.1063/1.3272536.
(59) Romanov, A. N.; Gularyan, S. K.; Polyak, B. M.; Sakovich, R. A.; Dobretsov, G. E.; Sarkisov, O. M. Electronically Excited States of Membrane Fluorescent Probe 4-Dimethylaminochalcone: Results of Quantum Chemical Calculations. *Phys. Chem. Chem. Phys.* **2011**, *13* (20), 9518-9524. DOI: 10.1039/C0CP02880K.
(60) Carlotti, B.; Elisei, F.; Mazzucato, U.; Spalletti, A. Unusual High Fluorescence of Two Nitro-Distyrylbenzene-like Compounds Induced by CT Processes Affecting the Fluorescence/Intersystem-Crossing Competition. *Phys. Chem. Chem. Phys.* **2015**, *17* (22), 14740-14749. DOI: 10.1039/C5CP00291E.
(61) Ghosh, R.; Nandi, A.; Palit, D. K. Solvent Sensitive Intramolecular Charge Transfer Dynamics in the Excited States of 4-N,N-Dimethylamino-4′-Nitrobiphenyl. *Phys. Chem. Chem. Phys.* **2016**, *18* (11), 7661-7671. DOI: 10.1039/C5CP07778H.
(62) Yang, W.; Zhao, J.; Sonn, C.; Escudero, D.; Karatay, A.; Yaglioglu, H. G.; Küçüköz, B.; Hayvali, M.; Li, C.; Jacquemin, D. Efficient Intersystem Crossing in Heavy-Atom-Free Perylenebisimide Derivatives. *J. Phys. Chem. C* **2016**, *120* (19), 10162-10175. DOI: 10.1021/acs.jpcc.6b01584.
(63) Lewis, F. D.; Lauterbach, R. T.; Heine, H. G.; Hartmann, W.; Rudolph, H. Photochemical Alpha Cleavage of Benzoin Derivatives: Polar Transition States for Free-Radical Formation. *J. Am. Chem. Soc.* **1975**, *97* (6), 1519-1525. DOI: 10.1021/ja00839a041.
(64) Gularyan, S. K.; Sarkisov, O. M.; Dobretsov, G. E.; Svetlichnyi, V. Y.; Gostev, F. E.; Antipin, S. A. 4-Dimethylaminochalcone as Fluorescent Probe: Effect of the Medium Polarity on Relaxation Processes in the Excited State. *Russ. Chem. Bull.* **2004**, *53* (8), 1670-1673. DOI: 10.1007/s11172-005-0015-z.
(65) Nagarajan, K.; Mallia, A. R.; Muraleedharan, K.; Hariharan, M. Enhanced Intersystem Crossing in Core-Twisted Aromatics. *Chem. Sci.* **2017**, *8* (3), 1776-1782. DOI: 10.1039/C6SC05126J.

(66) Stephansen, A. B.; Sølling, T. I. Distortion Dependent Intersystem Crossing: A Femtosecond Time-Resolved Photoelectron Spectroscopy Study of Benzene, Toluene, and p-Xylene. *Struct. Dyn.* **2017**, *4* (4). DOI: 10.1063/1.4977735.
(67) Rehm, D.; Weller, A. Kinetics of Fluorescence Quenching by Electron and H-Atom Transfer. *Isr. J. Chem.* **1970**, *8* (2), 259-271. DOI: 10.1002/ijch.197000029.
(68) Lakowicz, J. R. Quenching of Fluorescence. In *Principles of Fluorescence Spectroscopy*, Lakowicz, J. R. Ed.; Springer US, Boston, MA, 1983; pp 257-301.
(69) Sandanayaka, A. S. D.; Araki, Y.; Luo, C.; Fujitsuka, M.; Ito, O. Photoinduced Electron-Transfer Processes of Fullerene (C60) with Amine Donors: Excited Triplet Route vs Excited Singlet Route. *Bull. Chem. Soc. Jpn.* **2004**, *77* (7), 1313-1322. DOI: 10.1246/bcsj.77.1313.
(70) Peters, K. S.; Freilich, S. C.; Schaeffer, C. G. Dynamics of Electron Transfer in Amine Photooxidation. *J. Am. Chem. Soc.* **1980**, *102* (17), 5701-5702. DOI: 10.1021/ja00537a060.
(71) Devadoss, C.; Fessenden, R. W. Picosecond and Nanosecond Studies of the Photoreduction of Benzophenone by 1,4-Diazabicyclo[2.2.2]Octane: Characterization of the Transient. *J. Phys. Chem.* **1990**, *94* (11), 4540-4549. DOI: 10.1021/j100374a036.
(72) Demeter, A.; Biczok, L.; Berces, T.; Wintgens, V.; Valat, P.; Kossanyi, J. Laser Photolysis Studies of Transient Processes in the Photoreduction of Naphthalimides by Aliphatic Amines. *J. Phys. Chem.* **1993**, *97* (13), 3217-3224. DOI: 10.1021/j100115a025.
(73) Görner, H. Electron Transfer from Triethylamine to the Triplet State of Dinitronaphthalenes, 4,4'-Dinitrobiphenyl and 2,7-Dinitrofluorenone: Time Resolved UV–Vis Spectroscopic and Conductometric Study in Polar Solvents. *J. Phys. Chem. A* **2002**, *106* (25), 5989-5998. DOI: 10.1021/jp013754o.
(74) Hoffmann, N.; Görner, H. Photoinduced Electron Transfer from N-Methylpyrrolidine to Ketones and Radical Addition to an Electron-Deficient Alkene. *Chem. Phys. Lett.* **2004**, *383* (5), 451-455. DOI: 10.1016/j.cplett.2003.11.045.
(75) Chen, P.-Z.; Niu, L.-Y.; Chen, Y.-Z.; Yang, Q.-Z. Difluoroboron β-diketonate Dyes: Spectroscopic Properties and Applications. *Coord. Chem. Rev.* **2017**, *350*, 196-216. DOI: 10.1016/j.ccr.2017.06.026.